Extreme Mechanics Letters 12 (2017) 77–85

Contents lists available at ScienceDirect

Extreme Mechanics Letters

journal homepage: www.elsevier.com/locate/eml

Design of cut unit geometry in hierarchical kirigami-based auxetic metamaterials for high stretchability and compressibility

Yichao Tang, Jie Yin *

Applied Mechanics of Materials Laboratory, Department of Mechanical Engineering, Temple University, 1947 North 12th Street, Philadelphia, PA 19122, USA

ARTICLE INFO

Article history:
Received 2 March 2016
Received in revised form
5 July 2016
Accepted 15 July 2016
Available online 30 July 2016

Keywords:
Kirigami
Auxetic metamaterial
Hierarchy
High stretchability
Compressibility

ABSTRACT

We studied the mechanical response of a recently developed new class of mechanical metamaterials based on the paper art of cutting, kirigami. Specially, the geometrical and structural design of representative cut units, via combined line cut, cut-out, and hierarchy of the structure, was explored for achieving both extreme stretchability and/or compressibility in kirigami metamaterials through experiments, alongside geometrical modeling and finite element simulations. The kirigami design was tested on constituent materials including non-stretchable copy papers and highly stretchable silicone rubber to explore the role of constituent material properties. The cut unit in the shape of solid rectangles with the square shape as a special case was demonstrated for achieving the extreme stretchability via rigid rotation of cut units. We found that compared to the square cut units, the theoretically predicted maximum stretchability via unit rotation in rectangle units (aspect ratio 2:1) increased dramatically from about 41% to 124% for the level 1 cut structure without hierarchy, and from about 62% to 156% for the level 2 hierarchical cut structure, which was validated by both experiments and simulations. To demonstrate the achievement of both extreme stretchability and compressibility, we replaced the solid square cut units with porous squares and re-entrant lattice shapes in silicone rubber based metamaterials. We found that a porous structure can enable an extreme compressibility of as high as 81%.

1. Introduction

Mechanical metamaterials [1] are attracting increasing interest in scientific research and engineering innovation due to their unprecedented physical properties [2–7], arising from the geometrical arrangement of their periodic unit cells. Upon deformation, mechanical metamaterials can be reconfigured beyond their original designs [8–14], offering an enhanced flexibility in performance by coupling dynamically changing structural configurations with tunable physical properties [15].

Very recently, kirigami ("kiri" means cut), art of paper cutting, is becoming an emerging research frontier due to its broad potential applications in design of pluripotent materials [16,17], stretchable and conformable electronics [18], stretchable energy storage devices [19], optical tracking in solar cells [20], acoustic filters [21], and 3-D mesostructures fabrication [22]. By introducing hierarchical line cuts into thin sheets of elastomer, we and other researchers [18,23] showed that hierarchical cuts can generate highly stretchable, super-conformable, and ultra-soft reconfigurable metamaterials [18,23], which exhibit highly nonlinear stress–strain behaviors resulting from the hierarchically cut structure rather than their constituent material [23]. The underlying mechanism lies in the fact that stretching deformation in the cut structure is largely accommodated by the rigid rotation of cut units, rather than severely deforming the cut units themselves [18,23].

Despite the recent advancement, limitations and challenges remain. First, since the extraordinary properties in the cut-based metamaterials are mainly determined by the rotation of cut units [18,23], the order of rotational symmetry in the geometry of cut units will play an important role in determining the structural configuration governed mechanical behaviors of hierarchical kirigami metamaterials, including the extreme stretchability and tunable Poisson's ratio, which remain to be exploited. Second, the line cuts can only generate stretchable metamaterials [18,23]. The non-compressibility beyond their original cut configurations will largely hinder their potential applications in stretchable electronics [9] and other conditions, where both stretchability and compressibility are often experienced and required for functionality.

* Corresponding author.
E-mail address: jieyin@temple.edu (J. Yin).

http://dx.doi.org/10.1016/j.eml.2016.07.005
2352-4316/

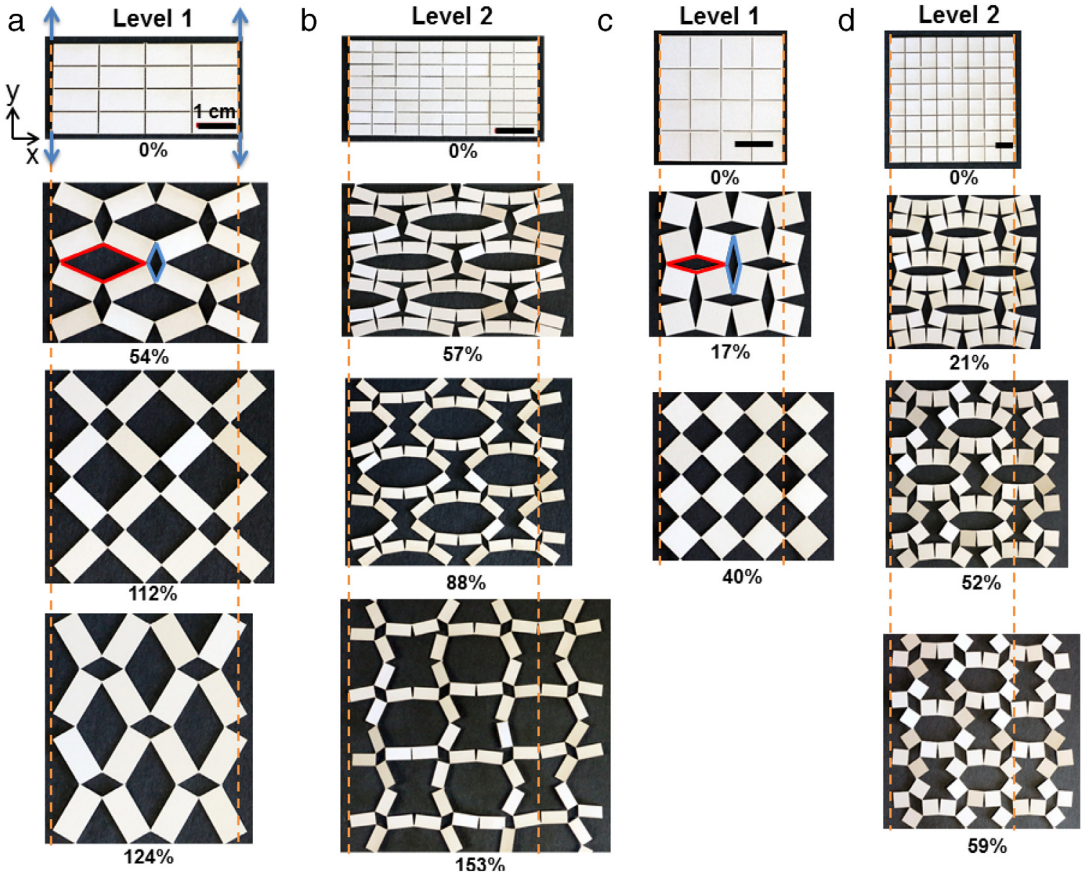

Fig. 1. Evolution of structural reconfiguration in hierarchical paper kirigami metamaterials constructed from rectangle (a–b) and square (c–d) cut units with the stretching along *y*-axis. (a) and (c): level 1 structure; (b) and (d): level 2 structure. (For interpretation of the references to color in this figure legend, the reader is referred to the web version of this article.)

Here, we first explore the design of a more generalized rectangular cut unit in hierarchical metamaterials for achieving the extreme stretchability through rigid rotation of cut units (Fig. 1(a)–(b)), where square cut units [18,23] will become a special case in this work. We find that compared to square units, rectangle cut units can significantly enhance their extreme stretchability by more than three folds (for the case of aspect ratio 2:1) depending on the shape anisotropy of rectangles, as well as greatly extend the stretching strain range for exhibited auxetic behavior. Furthermore, we study the combined line cuts and cut-outs to circumvent the limitation of non-compressibility in cut-based stretchable metamaterials. We find that in addition to the stretchability provided by line cuts, the cut-outs enable the compressibility upon compacting the cut-outs via buckling, allowing the realization of both stretchability and compressibility in one structure at the same time.

2. Stretchable hierarchical paper kirigami metamaterials: rectangular vs. square cut unit

Fig. 1(a) shows a level 1 kirigami metamaterial consisting of a thin sheet of copy paper with prescribed patterned cuts *via* a laser cutter, where orthogonal cuts divide a rectangle unit cell into 4 connected sub-squares and the aspect ratio of the rectangle m, i.e. the ratio of its length a to width b, is set to be 2. A hierarchical structure with self-similarity can be constructed by repeating the same cuts in each sub-level of the rectangular units, leading to a level 2 (Fig. 1(b)) and higher-level hierarchical structure. Similarly, when the aspect ratio m is set to be 1, i.e. $m = 1$, the rectangle shape reduces to square, generating a hierarchical square-cut unit based kirigami metamaterial (Fig. 1(c)–(d)).

As demonstrated in Fig. 1, stretching the kirigami structures vertically led to the lateral expansion, exhibiting an auxetic behavior with a negative Poisson's ratio. Upon stretching, each cut unit rotated around its hinges, i.e. the cut tip on its corner, to generate expandable structures. Upon stretching the level 1 structure, the line cuts in rectangle cut units evolved into orthogonal rhombus pores with both small (blue) and large sizes (red) (2nd row of Fig. 1(a)) whereas uniform pores in square cut units (2nd row of Fig. 1(c)). Both structures expanded laterally through the rotation of cut units. With further stretching, a polarization orientation switch from x to y axis was observed in the distribution of rhombus pores for rectangular cuts (4th row of Fig. 1(a)) but not in the case of square cuts (3rd row of Fig. 1(c)). Here the orientation is defined as the direction along the long diagonal of a large rhombus. A more complex evolution of pore shapes and sizes with the stretching strain was observed in level 2 structures (Fig. 1(b) and (d)).

Meanwhile, hierarchical cuts can make a non-stretchable and non-shearable paper sheet become highly stretchable through rigid rotation of cut units. The last row in each column of Fig. 1 shows the expanded structural configuration right before failure, i.e. the rupture of hinges. Fig. 2 summarizes the failure strain for both square and rectangle cut units based hierarchical metamaterials. It shows that either increasing the hierarchical level of cut structures or increasing the aspect ratio of cut units leads to an enhanced maximum stretchability. However, compared to increase the hierarchical level, increasing the aspect ratio m of cut units can dramatically enhance the maximum stretchability. When m was increased from 1 to 2, we observed an over three folds increase in the maximum stretchability in level 1 structure from

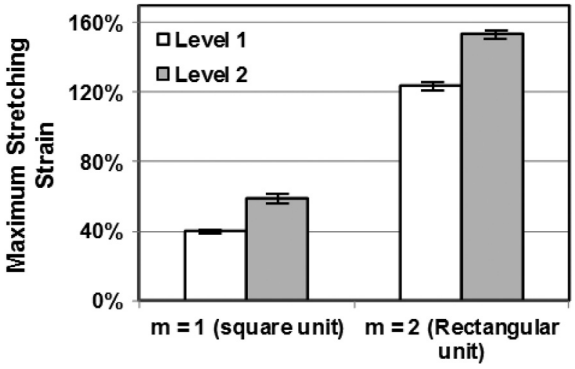

Fig. 2. Measured maximum stretchable strain in level 1 and level 2 paper kirigami metamaterials constructed from square and rectangle cut units.

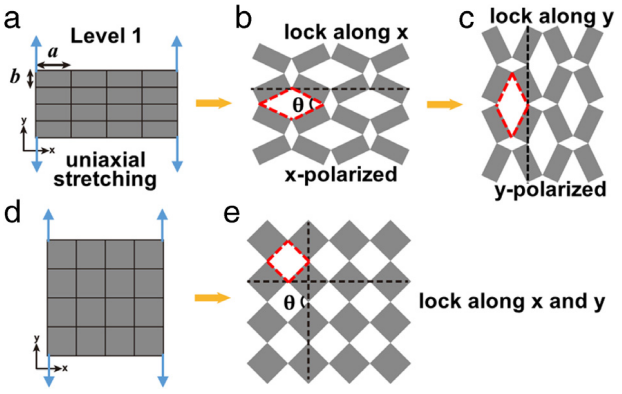

Fig. 3. (a–c) Schematic illustration of polarization switch from *x*-polarized (b) to *y*-polarized (c) in level 1 rectangle cut-unit based metamaterials with the increase of stretching along *y*-axis. *x*-polarized and *y*-polarized states correspond to a locked configuration with the maximum stretchability when the diagonal of cut units (dashed lines) aligns with *x*- and *y*-axis, respectively. (d–e) Schematic illustration of simultaneous polarization in both *x* and *y*-axis in level 1 square cut-unit based metamaterials with the increase of stretching along *y*-axis, showing the absence of polarization switch with a locked structural configuration in both directions (e).

about 40% in square units to about 124% in rectangle units. Similar two folds increase was found in the level 2 structures, showing the dramatic influence of cut unit geometries on the maximum stretchability of kirigami metamaterials.

3. Geometrical modeling of stretchable hierarchical kirigami metamaterials

To better understand the mechanical behavior of hierarchical paper kirigami metamaterials, we developed a geometrical model to predict both the auxetic behavior and the maximum stretchability observed in the experiments. In the geometrical modeling, each cut unit/subunit is assumed to be a rigid body and connected through hinges. The cut unit is assumed to rotate freely around its hinges with vanishing spring stiffness without considering the bending and stretching deformation in real materials and possible materials failure.

3.1. Level 1 cut structure

For level 1 structure (Fig. 3(a)), it has one degree of freedom and can be well defined by the opening angle (θ) in Fig. 3(b). The nominal strains of level-1 structure along the *x*- (ε_x^{Lvl-1}) and *y*-axis (ε_y^{Lvl-1}) can be given by:

$$\varepsilon_x^{Lvl-1} = \cos\left(\frac{\theta}{2}\right) + \frac{1}{m}\sin\left(\frac{\theta}{2}\right) - 1 \tag{1}$$

$$\varepsilon_y^{Lvl-1} = \cos\left(\frac{\theta}{2}\right) + m\sin\left(\frac{\theta}{2}\right) - 1. \tag{2}$$

The Poisson's ratio υ^{Lvl-1} can be readily given by

$$\upsilon^{Lvl-1} = -\frac{d\varepsilon_x^{Lvl-1}}{d\varepsilon_y^{Lvl-1}} = -\frac{d\varepsilon_x^{Lvl-1}/d\theta}{d\varepsilon_y^{Lvl-1}/d\theta} = \frac{\cos(\theta/2)/m - \sin(\theta/2)}{m\cos(\theta/2) - \sin(\theta/2)}. \tag{3}$$

From Eq. (3), it can be seen that when $m = 1$, i.e. square cut units, υ^{Lvl-1} is constant with $\upsilon^{Lvl-1} = -1$, which is independent of the stretching strain. However, for $m \neq 1$, υ varies with the opening angle θ, i.e. the applied stretching strain, demonstrating the large influence of the cut geometry on the auxetic behavior.

The observed polarization switch from *x*-axis to *y*-axis in the rectangle cut unit (Fig. 1(a)) implies that there must exist a maximum lateral strain during the transition, which can be obtained mathematically by finding the maximum value of nominal strain along the *x*-axis ε_x^{Lvl-1} in Eq. (1). $d\varepsilon_x^{Lvl-1}/d\theta = 0$ gives the opening angle $\theta_{x-\max}^{Lvl-1}$ at which the maximum lateral strain $\varepsilon_{x-\max}^{Lvl-1}$ occurs, i.e.

$$\theta_{x-\max}^{Lvl-1} = \pi - 2\tan^{-1}(m) \tag{4}$$

$$\varepsilon_{x-\max}^{Lvl-1} = \frac{2m}{\sqrt{m^2+1}} - 1. \tag{5}$$

Geometrically, the opening angle in Eq. (4) corresponds to a special geometrical configuration as shown in Fig. 3(b), where the diagonals of rectangle cut units will be in alignment with the *x*-axis. Physically, such a structural configuration is in a locked deformation state, which cannot be further stretched horizontally due to its infinite stiffness along the *x*-axis, thus, Eq. (5) represents the maximum stretchable strain through rigid rotation of cut units along the *x*-axis for the cut-structure. We refer this state as being *x*-polarized, which defines a critical transition state of zero Poisson's ratio in terms of Eq. (3) with $d\varepsilon_x^{Lvl-1}/d\theta = 0$, where the Poisson's ratio transits from an initial negative value to a positive value with the increase of applied stretching strain.

Since the uniaxial stretching strain is applied along the *y*-axis, the structural configuration in Fig. 3(b) can be further stretched vertically until the diagonals of rectangles become in alignment with the stretching direction, *y*-axis (Fig. 3(c)), where the structure will become locked along the *y*-axis, achieving its maximum stretchable strain ε_y^{Lvl-1} along the *y*-axis. The corresponding maximum opening angle θ_y^{Lvl-1} can be found either geometrically from the simple geometry of aligned diagonals as shown in Fig. 3(c) or mathematically from $d\varepsilon_y^{Lvl-1}/d\theta = 0$, which gives

$$\theta_{y-\max}^{Lvl-1} = \pi - \theta_{x-\max}^{Lvl-1} = 2\tan^{-1}(m) \tag{6}$$

$$\varepsilon_{y-\max}^{Lvl-1} = \sqrt{m^2+1} - 1. \tag{7}$$

Similarly, we refer the locked state at a strain of ε_y^{Lvl-1} as a *y*-polarized state, which also defines a critical state with an infinite Poisson's ratio in terms of Eq. (3) with $d\varepsilon_y^{Lvl-1}/d\theta = 0$.

From Eqs. (4)–(7), it can be seen that in the special case of $m = 1$, when $\theta = 90°$, the deformed structural configuration of square cut structures (Fig. 3(d)) will become locked along both directions of *x*- and *y*-axis simultaneously, where both diagonals happen to align with *x* and *y*-axis (Fig. 3(e)), respectively. Thus, the cut units cannot rotate any more and the structural configuration in Fig. 3(e) cannot be stretched through rigid rotation of cut units in both directions, which is consistent with the experiment as shown in the third row of Fig. 1(c) with $\theta = 90°$. The simultaneous deformation locking in both directions also explains the absence of the polarization switch observed in the case of level 1 square cut structure.

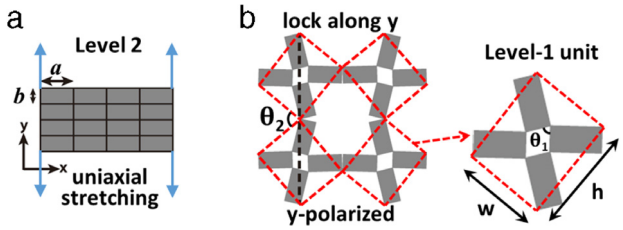

Fig. 4. Schematic illustration of a *y*-polarized and locked structural configuration along *y*-axis in level 2 rectangle cut-unit based metamaterials (a) at the maximum stretchable strain along *y*-axis (b). The level 2 is locked when the diagonal of virtual level-1 unit highlighted in red dashed lines aligns with the *y*-axis. (For interpretation of the references to color in this figure legend, the reader is referred to the web version of this article.)

3.2. Level 2 cut structure

For a level 2 cut structure (Fig. 4(a)), the number of degree of freedom becomes 2 and the geometry of the expanded structure can be well defined by the opening angle θ_1 in the level-1 unit, as well as the opening angle θ_2 in the virtual level-2 unit enclosed by red dashed lines as shown in Fig. 4(b). The size of the virtual rectangular level-2 unit depends on the rotation of level-1 cut units and thus will vary with θ_1. It should be noted that geometrically θ_1 and θ_2 are independent from each other. The nominal strains of a level 2 cut structure along *x*-axis (ε_x^{Lvl-2}) and *y*-axis (ε_y^{Lvl-2}) can be given by

$$\varepsilon_x^{Lvl-2} = \frac{w\cos(\theta_2/2) + h\sin(\theta_2/2)}{2a} - 1 \tag{8}$$

$$\varepsilon_y^{Lvl-2} = \frac{w\sin(\theta_2/2) + h\cos(\theta_2/2)}{2b} - 1 \tag{9}$$

where $w = 2a\cos(\theta_1/2)$ and $h = 2a\sin(\theta_1/2) + 2b\cos(\theta_1/2)$ are defined in Fig. 4(b) and $\theta_1 \le \theta_2$ must be satisfied. The Poisson's ratio can be given by

$$\upsilon^{Lvl-2} = -\frac{d\varepsilon_x^{Lvl-2}}{d\varepsilon_y^{Lvl-2}}. \tag{10}$$

Similar to the level 1 structure, when the structure becomes *y*-polarized upon increasing the stretching strain along the *y*-axis, i.e. geometrically, the diagonal in the virtual level-2 unit (enclosed by red dashed lines) is aligned with the *y*-axis (Fig. 4(b)), the structure arrives at a possible locked state along the *y*-axis. In this case, the nominal strain can be given by

$$\varepsilon_y^{Lvl-2} = \frac{\sqrt{w^2(\theta_1) + h^2(\theta_1)}}{2b} - 1. \tag{11}$$

The maximum value of Eq. (11) will correspond to the maximum stretchability $\varepsilon_{y-\max}^{Lvl-2}$ along the *y*-axis, i.e. the locked state. $d\sqrt{w^2(\theta_1) + h^2(\theta_1)}/d\theta_1 = 0$ gives the locked angle $\theta_{1-\max}^{Lvl-2} = \tan^{-1}(2m)$, and thus $\varepsilon_{y-\max}^{Lvl-2}$ is given by

$$\varepsilon_{y-\max}^{Lvl-2} = \frac{\sqrt{4m^2+1} - 1}{2}. \tag{12}$$

As seen from Eqs. (7) and (12), the maximum geometrically allowable stretchability in hierarchical cut-based metamaterials is only dependent on the aspect ratio of the rectangle cut units *m*, demonstrating the key role of the cut geometry in determining the stretchability.

4. Stretchable hierarchical kirigami metamaterials: experimental examination and numerical simulation

4.1. Maximum stretchability: non-stretchable paper materials

The geometrical modeling in Section 3 is first examined by comparing the measurements from paper-kirigami metamaterials in Fig. 1. The geometrical model (Eqs. (7) and (12)) shows an excellent agreement with the experiments in predicting the maximum geometrically allowable stretchability, which validates the model. For level 1 structure, the theoretical maximum stretchable strain along the *y*-axis is predicted to be 41.4% for square cut units ($m = 1$) and 123.6% for rectangle cut units ($m = 2$) from Eq. (7), which agree well with the corresponding measured maximum stretchable strain of 40% ± 1% for $m = 1$ and 124% ± 2% for $m = 2$ in paper kirigami metamaterials (Fig. 2). Similarly, for level 2 structure, the maximum stretchable strain predicted from Eq. (12) is 61.8% for $m = 1$ and 156.2% for $m = 2$, which also show an excellent agreement with the measured value of 59% ± 2% for $m = 1$ and 153% ± 3% for $m = 2$.

4.2. Maximum stretchability: highly stretchable elastomer materials

Despite the demonstrated excellent agreement of the rigid rotating model with paper kirigami structures, the discrepancy may originate when considering the emergent mechanical behavior contributed by the constituent material itself. We further examined the application of geometrical model to predict the mechanical behavior of hierarchical kirigami metamaterials consisting of hyperelastic materials through combined experiments and finite element method (FEM) simulation. Polydimethylsiloxane (PDMS) was chosen as base materials since it can withstand high-strain elastic deformation over 100%. The FEM simulation will be employed to provide important insights in understanding the polarization and deformation locking mechanism, as well as the critical deformation state close to hinge failure. In the FEM simulations, we will use the 3rd order Ogden model with inputs from measurements to model the hyperelastic behavior of PDMS. The procedures for sample preparation, experimental testing, and numerical simulations were described in details in our previous study [23], which will not be discussed here.

After introducing prescribed rectangular and square cuts to a 2 mm-thick thin sheet of PDMS through laser cutters, hierarchical PDMS metamaterials can be generated. The sheet was uniaxially stretched using an Instron tensile test machine until the structure began to rupture. Fig. 5 shows the representative structural configurations of level 1 and level 2 structures in the form of square ($m = 1$) and rectangle ($m = 2$) cut units at different applied stretching strains, which are well reproduced by the corresponding FEM simulations shown in Fig. 6(a) and (b). The evolution of structural reconfigurations (Figs. 5 and 6(a)–(b)) is similar to that in paper kirigami metamaterials (Fig. 1) since all the cut structures are reconfigured through the same mechanism of cut unit rotation.

The locked deformation at the polarization state observed in hierarchical PDMS and paper kirigami metamaterials is well captured by the FEM simulation in Fig. 6. Fig. 6(a) shows the same polarization switch from *x*-polarized (Fig. 6(a) (ii)) to *y*-polarized (Fig. 6(a) (iii)) configuration as Fig. 1(a) in the level 1 structure with rectangle cuts. Simulations show that when the structure is polarized along the *y*-axis, i.e. the diagonals of cut units (highlighted in red dashed line) are in alignment with the stretching direction of *y*-axis, the cut units will be ceased to rotate and thus the deformed structural configuration will be locked (Fig. 6(a) (iii)), as evidenced by the observed same structural configuration and the always upright diagonals upon further stretching (Fig. 6(a) (iv)), where only the connecting hinges

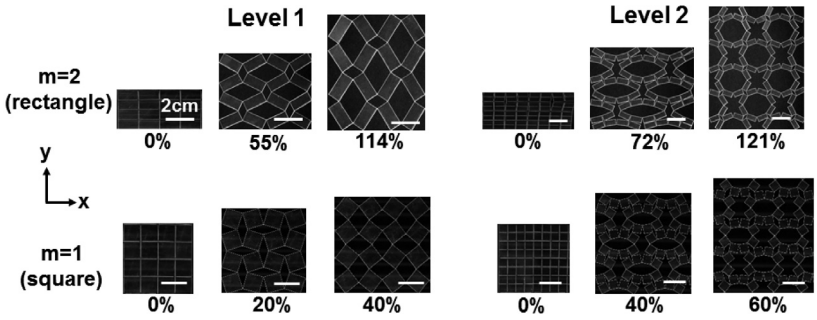

Fig. 5. Structural reconfiguration in hierarchical PDMS kirigami metamaterials constructed from rectangle (top row) and square cut units (bottom row) upon stretching along *y*-axis.

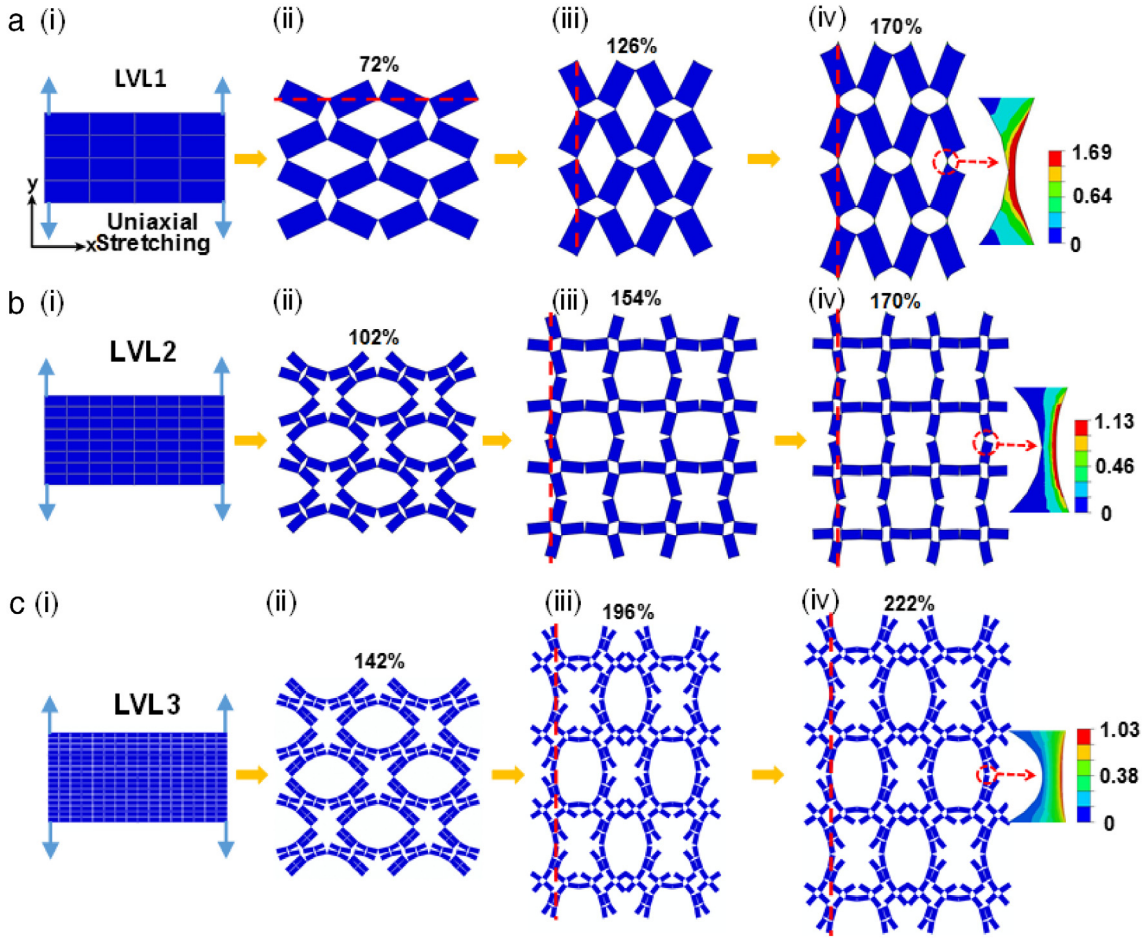

Fig. 6. FEM simulation results on structural reconfiguration and polarization in hierarchical PDMS kirigami metamaterials with rectangle cut units upon stretching along *y*-axis, where all figures show a simulated principal strain contour distribution. (a) Level 1 structure; (b) Level 2 structure; (c) Level 3 structure. Representative deformed configurations are shown at zero strain (Column 1), moderate strain (Column 2), locked strain (Column 3), and over-stretched strain beyond locked strain (Column 4) showing elongated hinges along *y*-axis. (For interpretation of the references to color in this figure legend, the reader is referred to the web version of this article.)

are being stretched and become elongated without the rotation of cut units to reconfigure the shape. Similar alignment of diagonals in cut units with the *y*-axis and locked structural configuration are observed in higher level of structures (e.g. level 2 in Fig. 6(b) (iii–iv) and level 3 in Fig. 6(c) (iii–iv)). The *y*-polarized and locked state defines the maximum stretchable strain through cut unit rotation, which is observed to increase dramatically from 126% in level 1 to 196% in level 3 from the FEM simulation, demonstrating the benefit of hierarchical cut structures in enhancing the extreme stretchability.

Fig. 7 shows the comparison of the maximum stretchable strain between the theory, experimental testing of both paper and PDMS materials, and FEM simulations of PDMS materials for level 1 and level 2 metamaterials with $m = 1$ and 2 in the cut units. It shows that the measured maximum stretchable strain in PDMS metamaterials is slightly lower than that predicted from the corresponding rigid rotation models for hierarchical square cut unit based metamaterials, whereas much lower (over 20%) for structures with rectangular cuts, especially for level 2 structures. It means that the structure undergoes failure earlier before reaching the theoretical maximum stretchable strain, which is reasonable since the severe stress concentration in the hinges (Fig. 6) will cause the hinges to rupture [23]. Despite the observed discrepancy from the experimental measurements, the maximum stretchable strain obtained from FEM simulations of PDMS kirigami metamaterials showed an excellent agreement

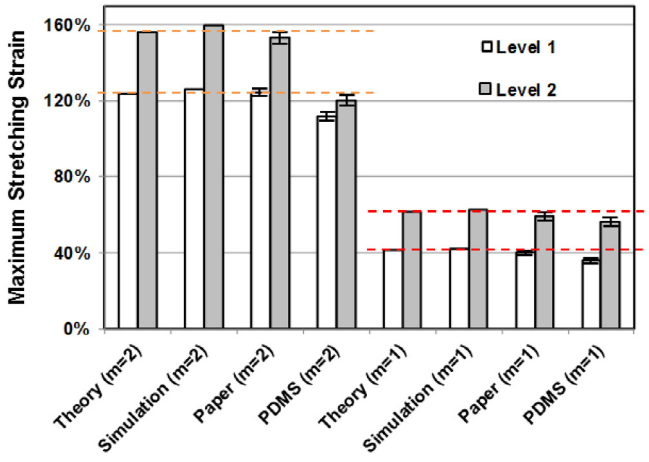

Fig. 7. Comparison of the maximum stretchable strain between theory, simulation, experiments (both paper and PDMS as the base materials) in the hierarchical kirigami metamaterials constructed from rectangle ($m = 2$) and square cut units ($m = 1$).

with the rigid rotation theory (Fig. 7), which validated the idealized geometrical model in Section 3.

4.3. Auxetic behavior: rectangle vs. square cut units

In addition to the large stretchability enabled by cuts, another important and interesting feature is the auxetic behavior of cut-based metamaterials. In this section, we will examine how the shape of cut units and the constituent material properties influence the auxetic behavior of cut-based hierarchical metamaterials.

Fig. 8 shows the comparison of Poisson's ratio as a function of nominal strain between the theory, experiment, and FEM simulation for hierarchical PDMS kirigami metamaterials constructed from rectangle ($m = 2$) and square ($m = 1$) cut units. For level 1 structure with $m = 2$, as the nominal strain increased from 0 to 120%, the Poisson's ratio predicted from Eq. (3) increased monotonically from -0.5 to 2 (Fig. 8(a)). The polarization switch from x-polarized to y-polarized state accounts for the switch from a negative to a positive Poisson's ratio. Specially, a zero Poisson's ratio is found at a strain of about 76%, indicating that the structure becomes x-polarized. Both experiment and FEM simulations show an excellent agreement with the rigid rotation based geometrical model, implying a negligible effect of constituent material properties on the Poisson's ratio in this case. However, a large discrepancy between the theory and experiment is observed for level 1 structure with $m = 1$ (Fig. 8(b)), especially when the applied strain is beyond 27%, where the Poisson's ratio from both experiments and FEM simulations starts to rise steeply and deviates from the theoretical prediction of a constant Poisson's ratio of -1. The reason is that the PDMS materials in the hinge areas undergo severe stretching when the applied strain is approaching to the lock strain.

For kirigami metamaterials with a higher hierarchical level, both experiments and FEM simulations show that the Poisson's ratio follows the similar trend as level 1 for both square and rectangle cut units (Fig. 8(c) and (d)), where the Poisson's ratio increases steeply when the applied nominal strain is approaching the lock strain since the Poisson's ratio will become infinite at the lock strain as discussed in Section 3. For example, as seen in both level 2 cut structures with $m = 1$ and $m = 2$, their Poisson's ratio–strain curves rise steeply when the applied strain is approaching to their respective lock strain of 61% ($m = 1$) and 156% ($m = 2$). Since the lock strain increases with the hierarchical level, the similar steep rise of Poisson's ratio–strain curves in higher hierarchical metamaterials will be expected to occur at a relatively larger applied strain (Fig. 8(c) and (d)), for example, a lock strain of 80% ($m = 1$) and 196% ($m = 2$) in the level 3 cut structure.

5. Both stretchable and compressible hierarchical kirigami metamaterials

The hierarchical kirigami metamaterials discussed so far still fall into the category of stretchable mechanical metamaterials, which cannot undergo in-plane compression beyond their original configuration (closed line cut state) due to the non-compressibility of line cuts. In this section, we will discuss the design of cut unit geometry through combined line cuts and cut-outs for achieving both stretchability and compressibility in hierarchical kirigami metamaterials.

5.1. Hierarchical porous-square-unit metamaterials

When we introduce circular cut-outs into the square units of the aforementioned hierarchical square cut unit based metamaterials (Fig. 9(a)), it will generate hierarchical porous kirigami metamaterials (with $r/a = 0.4$), for example, the level 1 and level 2 PDMS based porous metamaterials shown in the left of Fig. 9(c) and (d), respectively.

As seen in the middle of Fig. 9(c) and (d), increasing the hierarchical level of the porous cut structures can largely enhance the stretchability by opening lines cuts in both directions through rigid unit rotation. Upon uniaxially stretching the level 1 porous structure along the vertical direction (Fig. 9(c)), we observed that unlike the rigid rotation in the square cut units without pores, little rotation of porous cut units around hinges was observed since the vertical line cuts still remained closed. The porous square cut unit can no longer act as being a rigid body, which is easy to deform due to its largely reduced structural rigidity by the embedded pores. The stretching deformation of the structure was accommodated by directly stretching both the porous cut units and the horizontal line cuts as can be seen in the middle of Fig. 9(c), where both horizontal line cut and original circular pores were stretched to deform into an elliptical shape, leading to the monotonic increase of its Poisson's ratio from -1 to over 0.5 with the stretching strain (Fig. 9(b)). Thus, in this case, the stretchability of the whole structure will be mainly determined by the stretchability of its constituent materials rather than the structure, which should be avoided and is of no interest. However, when the level of the porous cut structure was increased to 2, we found that both horizontal and vertical line cuts at level 1 were largely opened to accommodate the vertical stretching through the rotation of sub-units at level 2 (middle of Fig. 9(d)), showing the advantage of a hierarchical structure. This leads to a similar Poisson's ratio–strain curve as the level 2 square cut metamaterials without pores (Fig. 9(b)). Little opening of the line cuts was observed in the sub-units at level 2, where they were subjected to slight deformation and the original circular pores deformed into ellipses with their long axis orthogonal to each other (middle of Fig. 9(d)). We envision that as the hierarchical level further increases, the pores in the sub-units at the higher level will also be opened to accommodate the stretching via unit rotation, and thus further enhance the stretchability of the porous cut hierarchical structures.

In addition to providing the stretchability through line cuts enabled rotation of cut units, the porous cut structure can also accommodate a large compression by compacting and closing its large volume of pores as show in the right of Fig. 9(c) and (d).

The right of Fig. 9(c) shows a highly compressed structural configuration of the level 1 porous cut structure under a uniaxial compressive strain of 50% along the vertical direction. It shows a similar buckled pattern as the porous membrane without

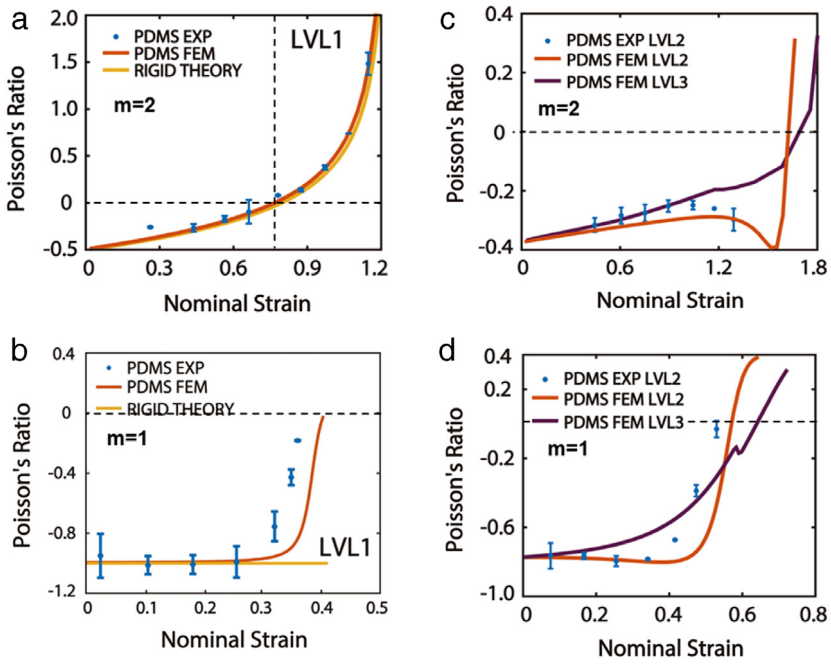

Fig. 8. Comparison of Poisson's ratio–strain curves between experiments, FEM simulations, and geometrical modeling for hierarchical PDMS kirigami metamaterials consisting of rectangle (a, c) and square (b, d) cut units upon uniaxial stretching at different hierarchical levels.

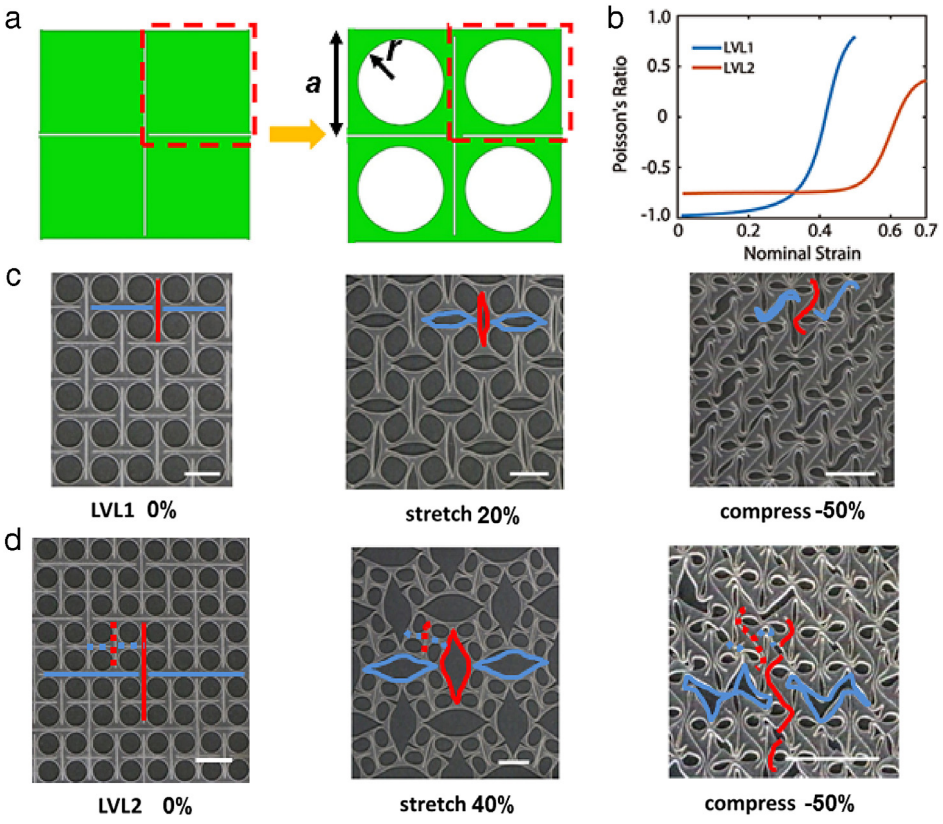

Fig. 9. (a) Schematic illustration of constructing both stretchable and compressible metamaterials by introducing circular cut-outs into the original solid square cut units with $r/a = 0.4$. (b) Simulated Poisson's ratio as a function of stretching strain of the correspondingly constructed level 1 and level 2 structures. (c–d) Experimental demonstrations of both stretchability and compressibility in level 1 (c) and level 2 (d) porous square cut based PDMS metamaterials upon stretching and compression. Scale bar is 2 cm. The shapes of representative line cuts are highlighted in red (vertical line cuts) and blue (horizontal line cuts) color before and after deformation. The dashed lines represent the line cuts in the 2nd level of subunits. In both (c) and (d), the optical images are scaled accordingly to show the details of the deformed structures. (For interpretation of the references to color in this figure legend, the reader is referred to the web version of this article.)

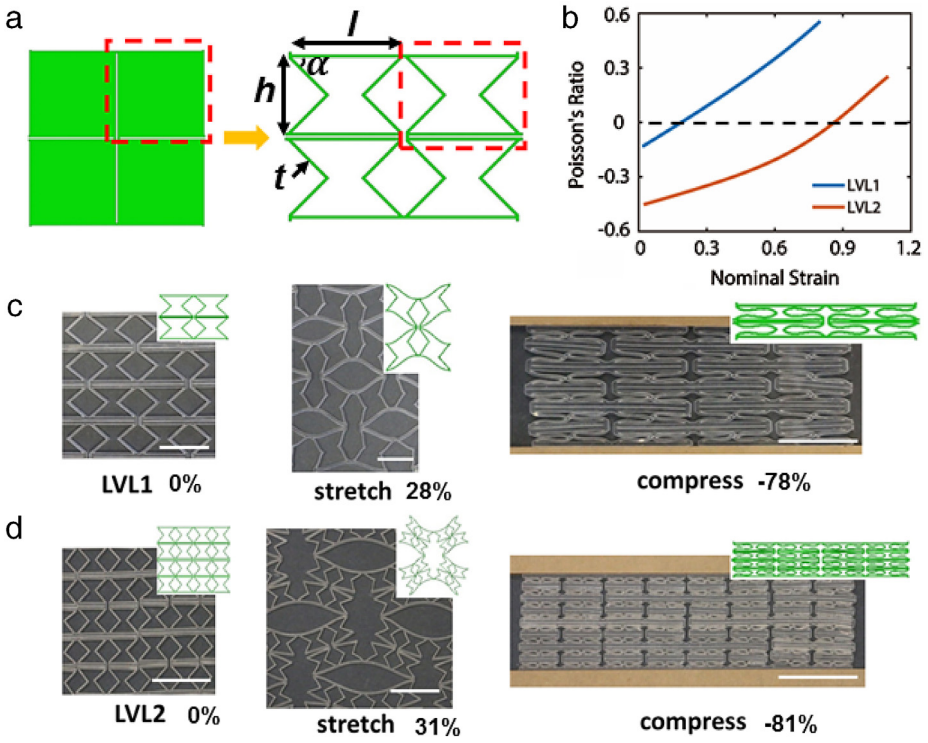

Fig. 10. (a) Schematic illustration of constructing both stretchable and compressible metamaterials by replacing square cut units with modified re-entrant lattice structures. (b) Simulated Poisson's ratio as a function of stretching strain of the correspondingly constructed level 1 and level 2 structures. (c–d) Experimental demonstrations of both stretchability and compressibility in level 1 (c) and level 2 (d) PDMS metamaterials constructed from re-entrant units upon stretching and compression. Scale bar is 2 cm.

introduced line cuts, the buckling of which under compression has been extensively studied [24,25]. The circular pores buckled into mutually orthogonal "8"-shaped pores. Both vertical (highlighted in red color) and horizontal (highlighted in blue color) line cuts were sheared and twisted at an approximate angle of 45° to the vertical direction due to its maximum shearing stress, where the vertical line cuts remained closed and deformed into an "S"-shaped line, whereas the horizontal line cuts were sheared and twisted into an open "S"-shaped slit.

A more complex buckling pattern was observed in the level 2 porous cut structure at a compressive stain of 50% as shown in the right of Fig. 9(d). Similar to the level 1 structure, all the pores buckled into arrays of orthogonal "8"-shaped pores. The original longer vertical line cuts at the 1st level (highlighted in red color solid lines) remained closed as lines but were deformed and broken into three line segments taking the shape of "C", "S", and "Ↄ", respectively, whereas the original longer horizontal line cuts at the 1st level (highlighted in blue color solid lines) were twisted to be open, forming a large "Z"-shaped pore. Similarly, the original longer vertical lines at the 2nd level (highlighted in red color dashed lines) were twisted into an "S"-shaped line, whereas the original shorter horizontal lines (highlighted in blue color dashed lines) were sheared to be an inclined slit at an approximate angle of 45° to the vertical direction.

Despite the demonstration of only one example of design, we envision that the volume ratio of the circular pores and different pore shapes can be manipulated to achieve the desired both compressibility and stretchability. The design of combined line cuts and cut-outs represents a category of compressible/stretchable metamaterials by introducing different shapes of pores into different geometries of cut units, which we believe can be readily applied to a variety of other shapes and structures.

5.2. Hierarchical re-entrant metamaterials

In principle, the way of achieving high stretchability through line cuts induced rigid rotation of units can be applied to any geometry of the cut unit. Since the key to design both stretchable and compressible metamaterials is to design the geometry of a cut unit, which can be largely compressible through in-plane deformation. The re-entrant geometry demonstrates both an extreme compressibility and auxetic behavior [26,27] upon compression, making it a good candidate for achieving compressibility. As one representative example, here, we use the modified re-entrant unit, which is highly compressible through buckling of beams, to replace the solid square unit in hierarchical square cut metamaterials (Fig. 10(a)) to demonstrate the concept of design. The modified re-entrant geometry can be characterized by the re-entrant angle α, height h, length l, and the thickness of beam t. Fig. 10(c) and (d) show the constructed level 1 and level 2 re-entrant structures consisting of PDMS materials, respectively, where $\alpha = 45^\circ$, $t = 0.25$ mm, $h = 10$ mm, and $l = 12.5$ mm.

The middle of the Fig. 10(c) and (d) shows the structural configuration at a uni-axial stretching strain of 28% and 31% along the vertical direction for level 1 and level 2, respectively. We found that the stretching behavior of re-entrant based hierarchical metamaterials is similar to that of the porous cut hierarchical ones in Fig. 9, where the stretching deformation of the structure is accommodated by directly stretching the beams in the re-entrant units for level 1 structure (middle of Fig. 10(c)), and nearly rigid rotation of re-entrant sub-units at the 2nd level for level 2 structure (middle of Fig. 10(d)), respectively. The stretched structural configurations with bended beams were well reproduced by the FEM simulations (insets of Fig. 10(c) and (d)). Correspondingly, the Poisson's ratio of the hierarchical structures was observed to increase monotonically from a negative to a positive value with the applied stretching strain.

Ideally, the re-entrant geometry can be fully compressed when $t/h \ll 1$ as can be seen from the nominal compressive strain equation of $\varepsilon_{re} = -(1 - 4t/h)$, achieving an extreme compressibility of 100%, which is independent of the hierarchical structures. The re-entrant hierarchical structures were shown to be compressed over 78% and 81% for level 1 (right of Fig. 10(c)) and

level 2 (right of Fig. 10(d)), respectively. We observed that all the original angled beams in both structures buckled into an "S" shape and became contacted with each other, exhibiting a zero Poisson's ratio without the lateral expansion of the structures observed, which is in contrast to the re-entrant based honeycomb [26,27] with a negative Poisson's ratio.

The modified re-entrant geometry represents a family of re-entrant hierarchical structures. We envision that the re-entrant angle, size, beam thickness, and the hierarchy level can be further manipulated to achieve the desired extreme compressibility through buckling of beams in the units and stretchability through unit rotation.

6. Conclusions

In summary, through combined experiments, geometrical modeling, and FEM simulations, we explored the design principles for achieving both extreme stretchability and/or compressibility in auxetic kirigami metamaterials via the combination of line cuts, cut-outs, and hierarchical structures: the line cuts enable the stretchability via rigid rotation of cut units, the cut-outs enable the compressibility via buckling induced full compactness of pores or lattices, and the hierarchical structural design enables the realization of extreme stretchability and/or compressibility. To demonstrate the design principles, we investigated the different geometries of representative cut units in a hierarchical structure, including solid rectangles with the square shape as a special case for demonstration of largely enhanced extreme stretchability via cut shapes, as well as squares with circular pores and re-entrant shapes for demonstration of achieving both stretchability and compressibility at the same time in a single structure. The design principle revealed in this work can be applied to a wide range of hierarchical kirigami based metamaterials with units in other geometrical shapes, including triangles, the more generalized parallelograms, and their combinations in the design of both solid and porous cut units with different pore shapes. We believe that this work can greatly expand the potential applications of kirigami metamaterials in conformable and stretchable electronics, biomedical devices, electronic skin, and reconfigurable soft robotics etc.

Acknowledgment

J. Y. acknowledges the funding support from the start-up at Temple University.

References

[1] J.-H. Lee, J.P. Singer, E.L. Thomas, Micro-/nanostructured mechanical metamaterials, Adv. Mater. 24 (36) (2012) 4782–4810.
[2] L. Fok, X. Zhang, Negative acoustic index metamaterial, Phys. Rev. B 83 (21) (2011) 214304.
[3] T. Brunet, et al., Soft 3D acoustic metamaterial with negative index, Nature Mater. 14 (4) (2015) 384–388.
[4] K.E. Evans, et al., Molecular network design, Nature 353 (6340) (1991) 124–124.
[5] S. Babaee, et al., 3D soft metamaterials with negative Poisson's ratio, Adv. Mater. 25 (36) (2013) 5044–5049.
[6] Z.G. Nicolaou, A.E. Motter, Mechanical metamaterials with negative compressibility transitions, Nature Mater. 11 (7) (2012) 608–613.
[7] T. Bückmann, et al., An elasto-mechanical unfeelability cloak made of pentamode metamaterials, Nature Commun. (2014) 5.
[8] H. Tao, et al., Reconfigurable terahertz metamaterials, Phys. Rev. Lett. 103 (14) (2009) 147401.
[9] J.P. Turpin, et al., Reconfigurable and tunable metamaterials: A review of the theory and applications, Int. J. Antennas Propag. 2014 (2014) 18.
[10] E. Hawkes, et al., Programmable matter by folding, Proc. Natl. Acad. Sci. 107 (28) (2010) 12441–12445.
[11] J.L. Silverberg, et al., Using origami design principles to fold reprogrammable mechanical metamaterials, Science 345 (6197) (2014) 647–650.
[12] J.L. Silverberg, et al., Origami structures with a critical transition to bistability arising from hidden degrees of freedom, Nature Mater. 14 (4) (2015) 389–393.
[13] S. Waitukaitis, et al., Origami multistability: From single vertices to metasheets, Phys. Rev. Lett. 114 (5) (2015) 055503.
[14] R. Gatt, et al., Hierarchical auxetic mechanical metamaterials, Sci. Rep. (2015) 5.
[15] A. Liu, et al., Micromachined tunable metamaterials: a review, J. Opt. 14 (11) (2012) 114009.
[16] D.M. Sussman, et al., Algorithmic lattice kirigami: A route to pluripotent materials, Proc. Natl. Acad. Sci. 112 (24) (2015) 7449–7453.
[17] T. Castle, et al., Making the cut: Lattice Kirigami rules, Phys. Rev. Lett. 113 (24) (2014) 245502.
[18] Y. Cho, et al., Engineering the shape and structure of materials by fractal cut, Proc. Natl. Acad. Sci. 111 (49) (2014) 17390–17395.
[19] Z. Song, et al., Kirigami-based stretchable lithium-ion batteries, Sci. Rep. 5 (2015) 10988.
[20] A. Lamoureux, et al., Dynamic kirigami structures for integrated solar tracking, Nature Commun. (6) (2015) 8092.
[21] V. Kunin, et al., Static and dynamic elastic properties of fractal-cut materials, Extreme Mech. Lett. 6 (2016) 103–114.
[22] Y. Zhang, et al., A mechanically driven form of Kirigami as a route to 3D mesostructures in micro/nanomembranes, Proc. Natl. Acad. Sci. 112 (38) (2015) 11757–11764.
[23] Y. Tang, et al., Design of hierarchically cut hinges for highly stretchable and reconfigurable metamaterials with enhanced strength, Adv. Mater. 27 (44) (2015) 7181–7190.
[24] G. Wu, Y. Xia, S. Yang, Buckling, symmetry breaking, and cavitation in periodically micro-structured hydrogel membranes, Soft Matter 10 (9) (2014) 1392–1399.
[25] K. Bertoldi, et al., Negative Poisson's ratio behavior induced by an elastic instability, Adv. Mater. 22 (3) (2010) 361–366.
[26] A. Alderson, K. Alderson, Auxetic materials, Proc. Inst. Mech. Eng. Part G: J. Aerosp. Eng. 221 (4) (2007) 565–575.
[27] W. Yang, et al., Review on auxetic materials, J. Mater. Sci. 39 (10) (2004) 3269–3279.